

Neurophotonics

Neurophotonics.SPIEDigitalLibrary.org

Red fluorescent proteins (RFPs) and RFP-based biosensors for neuronal imaging applications

Yi Shen
Tiffany Lai
Robert E. Campbell

Red fluorescent proteins (RFPs) and RFP-based biosensors for neuronal imaging applications

Yi Shen, Tiffany Lai, and Robert E. Campbell*

University of Alberta, Department of Chemistry, Edmonton, Alberta T6G 2G2, Canada

Abstract. The inherent advantages of red-shifted fluorescent proteins and fluorescent protein-based biosensors for the study of signaling processes in neurons and other tissues have motivated the development of a plethora of new tools. Relative to green fluorescent proteins (GFPs) and other blue-shifted alternatives, red fluorescent proteins (RFPs) provide the inherent advantages of lower phototoxicity, lower autofluorescence, and deeper tissue penetration associated with longer wavelength excitation light. All other factors being the same, the multiple benefits of using RFPs make these tools seemingly ideal candidates for use in neurons and, ultimately, the brain. However, for many applications, the practical utility of RFPs still falls short of the preferred GFPs. We present an overview of RFPs and RFP-based biosensors, with an emphasis on their reported applications in neuroscience. © 2015 Society of Photo-Optical Instrumentation Engineers (SPIE) [DOI: 10.1117/1.NPh.2.3.031203]

Keywords: red fluorescent protein; fluorescence imaging; genetically encoded biosensors; calcium ion; voltage; neurotransmitters.
Paper 14081SSR received Dec. 2, 2014; accepted for publication May 19, 2015; published online Jun. 19, 2015.

1 Red Fluorescent Proteins

Engineered fluorescent proteins (FPs) are the foundation of an indispensable toolbox for life science research that has revolutionized the ability of researchers to undertake real-time imaging of biomolecules in live cells. The current importance and ubiquity of FP-based techniques is discordant with the humble circumstances of the discovery of the first FP in the early 1960s. While extracting the bioluminescent protein Aequorin from *Aequorea victoria* jellyfish, Shimomura¹ noticed a second protein, *Aequorea victoria* green FP (avGFP), that gave “a very bright, greenish fluorescence.” In the following decades, advances in molecular biology facilitated the elucidation of the chromophore structure,² amino acid sequence, and gene sequence of avGFP.³ However, it was not until 1994 when the recombinant avGFP transgene was first used as a tool for molecular imaging. Specifically, it was used for visualization of gene expression in the worm *Caenorhabditis elegans*, thus demonstrating avGFP’s ability to fluoresce in cells from species other than jellyfish.⁴ Following this discovery, avGFP gained widespread acceptance as a revolutionary tool to visualize and track molecules and biochemical events in living cells and organisms. During the same period, improved variants of avGFP were engineered by manipulation and modification of the gene sequence.^{5–8} This resulted in creation of brighter green fluorescent variants^{6,8} and a number of variants with fluorescence maxima in the blue, cyan, green, and yellow regions of the visible spectrum.^{5,7} An avGFP variant that emits red fluorescence has been reported, but it is not bright enough to be practically useful for live cell imaging.⁹

One of the most significant advances following the cloning and recombinant expression of the avGFP transgene was the discovery of cyan, green, yellow, and red avGFP homologues in nonbioluminescent reef corals and sea anemones.¹⁰ The first

reef coral-derived red FP (RFP) to be extensively studied and engineered was isolated from the sea anemone *Discosoma* sp. This RFP, originally designated as drFP583 but more commonly known as DsRed,¹¹ has an excitation wavelength maximum (λ_{ex}) at 558 nm and an emission wavelength maximum (λ_{em}) at 583 nm. Unfortunately, DsRed has a very slow maturation rate ($t_{0.5} > 10$ h) and a substantial fraction of the protein molecules form a dead-end green fluorescent chromophore. The green product limits the utility of DsRed for multicolor imaging experiments with green fluorescent protein (GFP) variants.¹² More critically, DsRed is an obligate tetramer with a tendency to form even higher order oligomers. Accordingly, any target protein fused to DsRed becomes tetrameric itself. This artificial “tetramerization” can disrupt the native localization of the target protein and, particularly in cases where the target protein is itself an oligomer, lead to protein aggregation.^{13,14} These drawbacks limit the applications of wild-type DsRed for imaging of subcellular structures and protein localization and served as the impetus for the engineering of a monomeric version.

1.1 Monomerization of RFPs

Through the use of protein engineering, tetrameric DsRed was converted into monomeric RFP 1 (mRFP1; $\lambda_{ex} = 584$ nm; $\lambda_{em} = 607$ nm).¹⁵ In the DsRed tetramer, each subunit is engaged in distinct contacts with two of the other three subunits via two different interaction surfaces (Fig. 1). In order to monomerize DsRed, the protein–protein contacts at each interface were destabilized through mutations to charged residues such as lysine and arginine. Disruption of one interface yielded a dimeric intermediate and subsequent disruption of the remaining interface produced the monomeric FP (Fig. 1). While this process had the desirable outcome of producing monomeric variants,

*Address all correspondence to: Robert E. Campbell, E-mail: robert.e.campbell@ualberta.ca

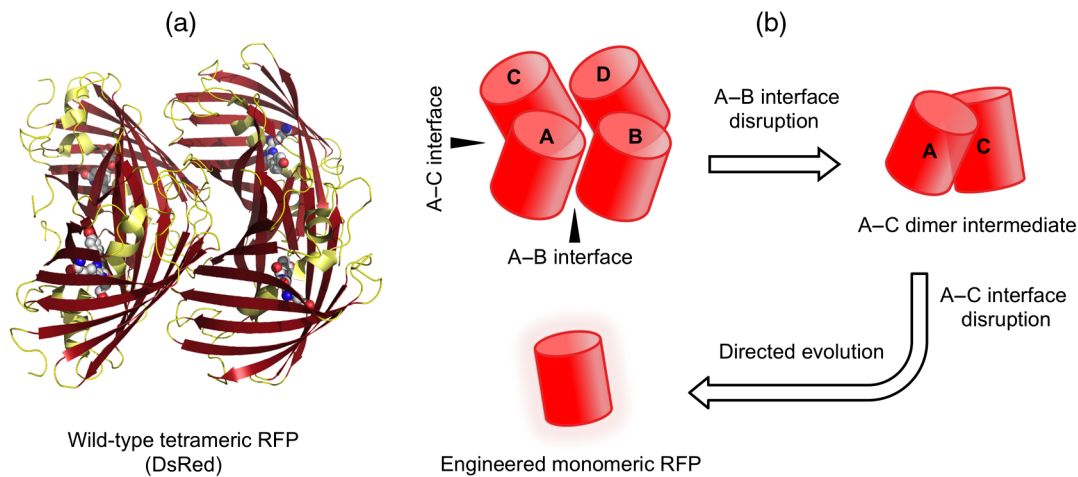


Fig. 1 Conversion of the wild-type tetrameric red fluorescent protein (RFP) DsRed to an engineered monomeric RFP. (a) Cartoon representation of the structure of wild-type tetrameric RFP DsRed. (b) Disruption of the first A–B interface produces an A–C dimer intermediate and subsequent disruption of the A–C interface produces a monomeric RFP. Interface-disrupting mutations are typically detrimental to the proper folding and chromophore maturation of the intermediate dimer or monomer; therefore, these variants must be rescued by directed evolution. Cartoon structures are based on PDB ID 1G7K.¹⁴

it also had the undesirable outcome of decreasing the intrinsic fluorescent brightness. A total of 33 mutations were introduced during the course of engineering mRFP1, including 13 interface-disrupting mutations and 20 fluorescence-rescuing mutations.¹⁶

The monomeric nature of mRFP1 addresses the most critical shortcoming associated with tetrameric DsRed. Other favorable properties of mRFP1 include a much shorter maturation time ($t_{0.5} < 1$ h) and a 25-nm red-shifted fluorescence emission at 607 nm. These advantages make mRFP1 suitable for the construction of fusion proteins for live cell fluorescence imaging, as well as in the multicolor fluorescence imaging with avGFP variants.¹⁵ Unfortunately, mRFP1 also exhibits disadvantages such as reduced fluorescence brightness and photostability. Efforts to further improve mRFP1 focused on higher brightness, color diversification, and improved photostability. These efforts eventually produced a number of useful RFP variants that are now known as the mFruit series.^{16,17} The prototypical RFP in the mFruit series is mCherry, which is generally considered to be the successor of mRFP1.

1.2 Structure and Chromophore Formation in RFPs

The x-ray crystal structures of DsRed and mCherry (as examples of prototypical RFPs) reveal that these proteins have a cylindrical shape created by eleven β -strands wrapped around a central helix.¹⁸ This distinctive tertiary structure, which is shared with avGFP,^{13,14,19,20} is often referred to as a β -can or a β -barrel. The β -barrel is ~ 4 nm in height and ~ 3 nm in diameter (Fig. 2). The chromophore is located near the middle of the central helix and is protected from the external environment by the eleven β -strands that surround it.

DsRed forms its chromophore from three sequential amino acids: Gln65, Tyr66, and Gly67.¹¹ There have been several reports of investigations into the mechanism of chromophore formation.^{11,21,22} The currently preferred proposed mechanism invokes a branched pathway that can lead to either green or red chromophores.²³ In this branched mechanism, the formation

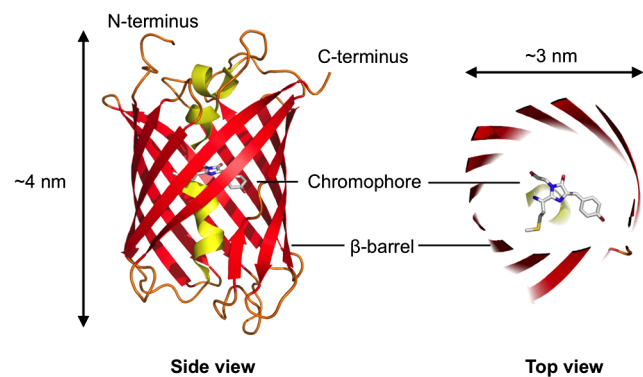


Fig. 2 Structure of a representative monomeric RFP, mCherry. The secondary structure is shown in a cartoon representation with the helix colored in yellow, β -strands colored in red, and loops colored in orange. The chromophore is shown in a stick representation with carbon atoms colored in gray, nitrogen atoms colored in blue, and oxygen atoms colored in red (PDB ID 2H5Q).

of the chromophore starts with the cyclization of the main chain to form a five-membered ring intermediate. This five-membered ring intermediate undergoes an initial step of oxidation to form a hydroxylated cyclic imine, which equilibrates with a cyclic imine. At this point, the mechanism branches. One branch results from the dehydration of the hydroxylated cyclic imine and leads to formation of the green fluorescent chromophore. On the other branch, irreversible oxidation of the cyclic imine leads to an intermediate with blue fluorescence. Further dehydroxylation and dehydration lead to formation of the red fluorescent chromophore of DsRed (Fig. 3).^{23,24} Insight into the mechanism of formation of the RFP chromophore, and the influence of its local environment on its spectral properties, opens new avenues for engineering FPs. Accordingly, a variety of RFP-derived colors have been engineered through engineering of the chromophore structure and its immediate environment, as will be described below.

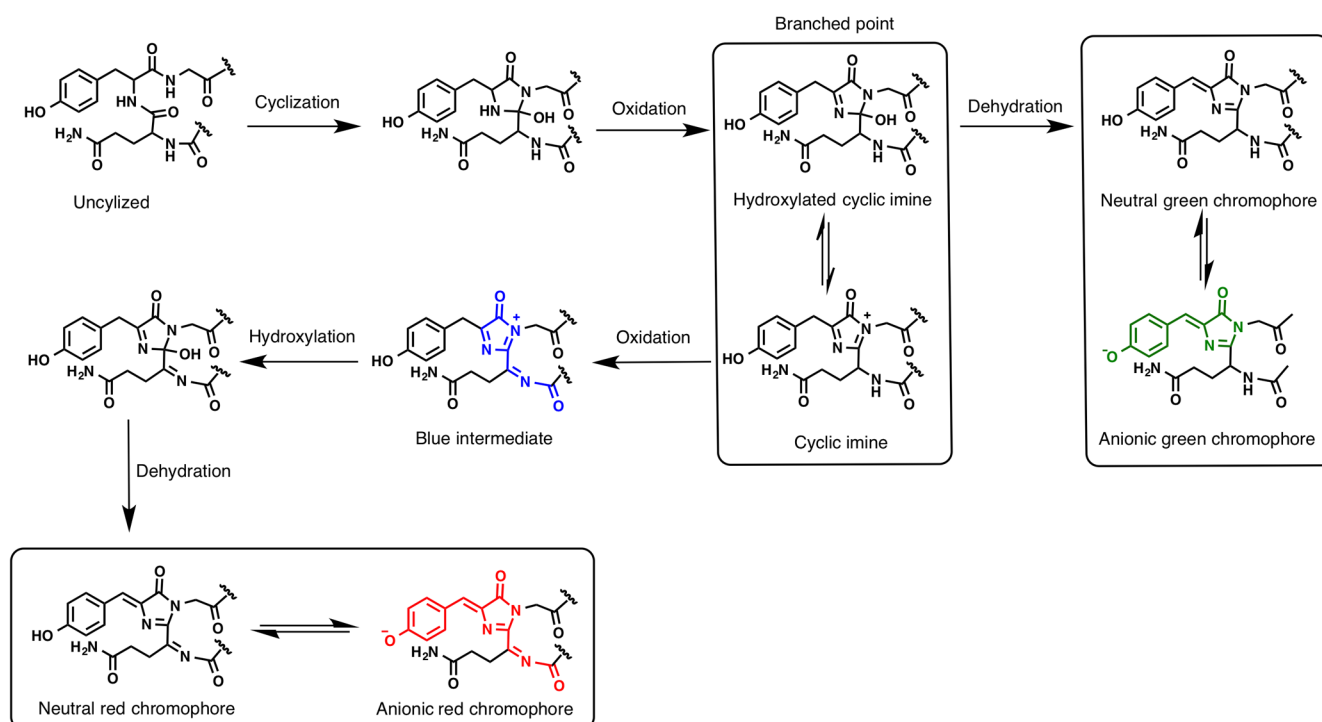


Fig. 3 Branched pathway mechanism for red chromophore formation (and dead-end green chromophore formation) in DsRed.

1.3 Classification of RFPs

FPs are now available in a wide range of colors spanning the visible spectrum.^{25–27} Relative to the more blue-shifted FPs, RFPs have a number of inherent advantages. Specifically, they are spectrally distinct from the commonly used avGFP variants, which makes them particularly useful for multicolor imaging applications. In addition, red-shifted fluorescence is associated with reduced background autofluorescence, lower phototoxicity, and better tissue penetration due to lower absorption.^{15,16,28} All other factors being the same, these properties should make RFPs superior probes for fluorescence imaging, particularly for *in vivo* applications.

Before further discussing RFPs and RFP-based biosensors, it is important to mention that all of the widely used FPs are the products of a combination of rational design and directed evolution. Engineering by rational design involves making changes to the amino acid sequence using insights derived from inspection of high-resolution protein structures, possibly supplemented with additional insights obtained from computer modeling. In practice, rational design alone rarely results in useful new FPs due to unanticipated negative effects, such as diminished protein folding efficiency. By contrast, directed evolution does not require prior information on the protein structure. Instead, random mutagenesis is carried out on the gene encoding the protein-of-interest to produce large libraries of mutants, which are then screened for variants with the desired properties. The power of directed evolution for protein engineering is well established but suffers from being relatively labor intensive and requiring an effective screening protocol. This approach may also lead to the accumulation of multiple “silent” mutations in addition to the beneficial ones. Nonetheless, the thoughtful combination of both strategies has significantly benefited not only the engineering of

RFPs and RFP-based biosensors but also essentially all of the FP variants currently available.

For the sake of this review, we have categorized RFPs into three classes based on their fluorescence spectral profiles. These three classes are standard RFPs (i.e., short Stokes shift with emission maxima in the 550 to 620 nm range), far RFPs (i.e., emission maxima at >620 nm), and long Stokes shift (LSS) RFPs (Table 1). Phototransformable RFPs including photoactivatable RFPs,²⁹ photoswitchable RFPs,^{30,31} and photoconvertible RFPs³² will not be further discussed in this review.³³ It is important to note that the blanket designation of all of these proteins as “red” is misleading, since many of them emit wavelengths of light that would appear orange to the naked eye.

1.4 Standard RFPs

The class of standard RFPs can be further subdivided into the “orange” RFPs with emission maximum at 550 to 580 nm and the “red” RFPs with emission maximum at 580 to 620 nm. One of the most important advances in generating standard RFPs in the orange and red spectral regions occurred during further evolution of mRFP1. Gln66, the first amino acid in the chromophore-forming tripeptide, is a critical determinant of the spectral profile of mRFP1 derivatives. For example, the Gln66Met mutation of mRFP1.1 and mCherry ($\lambda_{\text{ex}} = 587$ nm; $\lambda_{\text{em}} = 610$ nm) causes a slight red shift in the excitation and emission relative to mRFP1. Mutation of Gln66 to Cys or Thr was found to cause a blue shift in fluorescence. This observation inspired the development of mTangerine ($\lambda_{\text{em}} = 585$ nm; Gln66Cys), mOrange ($\lambda_{\text{em}} = 562$ nm; Gln66Thr) and mStrawberry ($\lambda_{\text{em}} = 596$ nm; Gln66Thr).

The gene for the brightly fluorescent dimeric intermediate created during the process of DsRed monomerization was

Table 1 Properties of selected red fluorescent protein (RFPs).

Protein	λ_{ex} (nm)	λ_{em} (nm)	EC	QY	Brightness	pK_a	Bleaching (s)	Maturation (min)	Reference
Standard RFPs									
mOrange	548	562	71000	0.69	49	6.5	9	150	16
mOrange2	549	565	58000	0.60	34.8	6.5	N.D.	N.D.	17
TagRFP	555	584	100000	0.48	49	3.8	48	100	34
TagRFP-T	555	584	81000	0.41	33.2	4.6	337	100	17
mRuby	558	605	112000	0.35	39.2	4.4	N.D.	N.D.	35
mRuby2	559	600	113000	0.38	43	5.3	123	150	36
mTangerine	568	585	38000	0.30	11.4	5.7	N.D.	N.D.	16
mApple	568	592	75000	0.49	36.7	6.5	N.D.	N.D.	17
mStrawberry	574	596	90000	0.29	26.1	4.5	15	50	16
FusionRed	580	608	95000	0.19	18.1	4.6	150	130	37
mCherry	587	610	72000	0.22	15.8	4.5	96	40	16
Far RFPs									
mKate	588	635	31500	0.28	8.8	6.2	N.D.	N.D.	38
mKate2	588	633	62500	0.40	25	5.4	84	20	39
mPlum	590	649	41000	0.10	4.1	4.5	53	100	40
mRaspberry	598	625	86000	0.15	12.9	N.D.	N.D.	N.D.	40
mNeptune	600	650	67000	0.20	13.4	5.4	255	35	28
TagRFP657	611	657	34000	0.10	3.4	5	N.D.	N.D.	41
TagRFP675	598	675	46000	0.08	3.7	5.7	N.D.	25	42
mCardinal	604	659	87000	0.19	16.5	5.3	730	27	43
Long Stokes shift (LSS) RFPs									
mKeima	440	620	14400	0.24	3.5	6.5	N.D.	N.D.	44
mBeRFP	446	611	65000	0.27	17.6	5.6	N.D.	N.D.	45
LSSmKate2	460	605	26000	0.17	4.4	2.7	N.D.	N.D.	46
LSSmKate1	463	624	31200	0.08	2.5	3.2	N.D.	N.D.	46
LSSmOrange	437	572	52000	0.45	23.4	5.7	N.D.	138	47

Note: EC: extinction coefficient; QY: quantum yield; brightness: the product of EC and QY; pK_a : pH value at which the fluorescence intensity is 50% of maximal; bleaching: time for fluorescence intensity to be photobleached by 50% under arc-lamp illumination; maturation: time for fluorescence intensity to reach 50% maximal upon exposure to oxygen; N.D.: not determined.

fused to a second copy of itself to create a “tandem dimer” RFP termed tdTomato ($\lambda_{\text{ex}} = 554$ nm and $\lambda_{\text{em}} = 581$ nm). Due to the formation of an intramolecular pseudodimer, tdTomato behaves like an exceptionally bright monomeric RFP, making this a popular tool for many applications.¹⁶

Later RFP engineering efforts focused on improving the photostability of the mFruit variants. Such efforts led to the production of mOrange2 ($\lambda_{\text{ex}} = 549$ nm and $\lambda_{\text{em}} = 565$ nm) with a

25-fold increase in photostability relative to mOrange.¹⁷ Due to their high brightness and photostability, mOrange and mCherry are generally the mFruit FPs of choice for live cell fluorescence imaging experiments when orange or red fluorescence is required. Several of the other mFruit FPs, including mTangerine and mStrawberry, are not often used for imaging as they suffer from low intrinsic brightness and poor photostability.

In addition to the DsRed-derived monomeric variants, a second lineage of standard monomeric RFPs was engineered from the sea anemone *Entacmaea quadricolor* RFPs eqFP578 and eqFP611.^{48,34} For example, TagRFP ($\lambda_{\text{ex}} = 555$ nm; $\lambda_{\text{em}} = 584$ nm) is a bright monomeric RFP engineered from the dimeric RFP eqFP578.³⁴ The Ser158Thr variant of TagRFP, designated as TagRFP-T, has improved photostability by approximately nine-fold.¹⁷ Another member of the eqFP578 variant family is FusionRed ($\lambda_{\text{ex}} = 580$ nm and $\lambda_{\text{em}} = 608$ nm), which exhibits decreased cytotoxicity when expressed in mammalian cells.³⁷ The eqFP611 lineage has also yielded mRuby ($\lambda_{\text{ex}} = 558$ nm and $\lambda_{\text{em}} = 605$ nm) and the brighter mRuby2 variant ($\lambda_{\text{ex}} = 559$ nm and $\lambda_{\text{em}} = 600$ nm), which exhibit a relatively LSS (~ 50 nm) between the excitation and emission maxima.^{35,36}

Although a growing number of engineered standard, far, and LSS RFPs have an “m” (as an abbreviation for monomeric) in front of their name, many do not behave as monomers when expressed in cells.⁴⁹ In some cases, the protein may form dimers or higher order oligomers, which can lead to aggregation and/or cytotoxicity.³⁷ Yet other RFPs, many of which are unambiguously monomeric, can form bright puncta in certain cells types due to accumulation in lysosomes or autophagosomes.^{50,51}

1.5 Far RFPs

Far RFPs with an emission maximum over 620 nm are of particular importance for *in vivo* and deep-tissue imaging in small animal models such as mice and rats. The spectral region between 600 and 1200 nm, bounded at the low wavelength by hemoglobin absorption and at the long wavelength by the increasing absorption of water, is known as the near-infrared “optical window.” This “optical window” has motivated FP engineers to push the excitation and emission wavelengths of RFP into the far-red and even the near infrared region.²⁸

Early efforts in creating further red-shifted RFPs from mRFP1 yielded mPlum ($\lambda_{\text{ex}} = 590$ nm and $\lambda_{\text{em}} = 649$ nm), mRaspberry ($\lambda_{\text{ex}} = 598$ nm and $\lambda_{\text{em}} = 625$ nm),⁴⁰ and mGrape ($\lambda_{\text{ex}} = 608$ nm and $\lambda_{\text{em}} = 646$ nm).²⁸ mCherry has also served as a template for the engineering of longer wavelength emission with the aid of a computationally designed library.⁵² This effort led to the creation of mRouge with a relatively long wavelength emission (maximum at 637 nm) but relatively low brightness (quantum yield of 0.03). Generally speaking, the far RFPs derived from DsRed are relatively dim and have not proven particularly useful for *in vivo* applications.

Entacmaea quadricolor lineage has served as a more promising source of far RFPs than the DsRed lineage. For example, the eqFP578-derived mKate ($\lambda_{\text{ex}} = 588$ nm and $\lambda_{\text{em}} = 635$ nm), mKate2 ($\lambda_{\text{ex}} = 588$ nm and $\lambda_{\text{em}} = 633$ nm), and mNeptune ($\lambda_{\text{ex}} = 600$ nm and $\lambda_{\text{em}} = 650$ nm) variants were engineered to exhibit bright far-red emission above 630 nm.^{28,38,39} Further efforts led to the development of two additional bright far-red mKate derivatives, mCardinal⁴³ and TagRFP657.⁴¹ These variants have excitation maxima of 604 and 611 nm, respectively, and 659-nm emission maxima for both. To date, the most red-shifted emission maximum for an RFP is 675 nm for the mKate variant TagRFP675.⁴²

1.6 LSS RFPs

LSS typically refers to fluorophores for which the difference between the fluorescence excitation and emission maxima is

larger than ~ 100 nm. The availability of LSS FPs provides researchers with a greater selection of spectrally resolvable colors for multicolor imaging application. LSS RFPs absorb blue light (usually in the range of ~ 440 to 460 nm) and fluoresce in the red region of the visible spectrum. They hold particular promise for two-photon fluorescence excitation due to the fact that they can be excited at the same two-photon wavelength as enhanced GFP (EGFP) using widely available pulsed laser systems.

The first reported LSS RFP, known as mKeima, was developed from a chromoprotein from the stony coral *Montipora* sp.⁴⁴ Later efforts were aimed at developing new LSS RFPs from standard and far RFPs. For example, three new LSS RFPs, LSSmKate1, LSSmKate2,⁴⁶ and mBeRFP⁴⁵ were engineered by providing an excited state proton transfer (ESPT) pathway for the mKate chromophore. Blue light excitation causes the chromophore to enter the excited state, which is associated with a decreased pK_a for the phenol group of the chromophore. Accordingly, following excitation of the neutral chromophore, the proton is transferred through the hydrogen bonds of the ESPT pathway to generate the lower energy excited state anionic state, which then emits red fluorescence.

LSSmKate1 and LSSmKate2 outperform mKeima in terms of pH-stability, photostability, and brightness. Unlike mKeima and mBeRFP, LSSmKates lack the additional excitation peak associated with the anionic ground state of the red chromophore (i.e., normal Stokes shift red fluorescence) at around 560 nm. The lack of this peak facilitates their combined use with standard RFPs in multicolor fluorescence imaging. The strategy of engineering ESPT pathways into standard RFPs has also been applied to some of the mFruit RFPs, including mOrange and mCherry, to generate variants with blue-shifted fluorescence excitation.⁵³ Further development produced LSSmOrange, which exhibits the highest brightness among all the LSS RFPs.⁴⁷

2 RFP-Based Biosensors

For monitoring of transcription and/or translation, visualization of organelles and other subcellular structures, and imaging of biomolecule motility and dynamics, the FP has a “passive” role.^{54,55} For many other applications, the FP is designed to play an “active” role, meaning that its inherent fluorescence intensity or hue will change in response to a specific cellular process of interest. These “active” FP constructs are interchangeably referred to as biosensors, sensors, indicators, or reporters. Examples of such FP-based biosensors include ones for intracellular pH,^{56–59} concentration of various ions,⁶⁰ second messengers such as ATP,⁶¹ redox potential,⁶² membrane voltage,⁶³ reactive oxygen species,⁶⁴ and various enzyme activities.⁶⁵ The utility of these biosensors can be extended by combining them with specific promoters and/or targeting signals for specific organelles, cells, or tissues, for either *in vitro* or *in vivo* applications.

Needless to say, the inherent advantages associated with RFPs (i.e., reduced autofluorescence, reduced phototoxicity, and deeper tissue imaging) extend to RFP-based biosensors. As will be described in the following sections, the last decade has seen an increasing number of examples of researchers taking an established GFP-based biosensor and converting it to a red fluorescent homologue. While the resulting biosensor does have the inherent advantage of red shifted fluorescence, it often has other drawbacks that can limit its real-world performance relative to its green fluorescent brethren.

2.1 Classification of RFP-Based Biosensors

Biosensors are generally composed of two parts: a molecular recognition/binding element that interacts with the target and a signal-transducing element that converts the interaction into a detectable signal, such as fluorescence. Several approaches have been employed to convert RFPs into effective signal-transducing elements for a variety of recognition events. Based on the design strategies employed, RFP-based biosensors can be categorized into four main classes: FP complementation-based biosensors, Förster resonance energy transfer (FRET)-based biosensors, dimerization-dependent FP (ddFP)-based biosensors, and single FP-based biosensors.

2.2 RFP Biosensors Based on Complementation

Complementation-based biosensors are based on the interaction-induced reassembly of a complete and functional FP from two (or more) nonfunctional fragments. To use FP complementation to visualize a protein–protein interaction, one FP fragment is genetically fused to one gene of an interacting protein pair and the other fragment is fused to the other gene of the pair. Before complementation, both of the fragments are partially or fully unfolded and nonfluorescent. Interaction of the two fused partners brings the nonfluorescent FP fragments into close proximity and enables the formation of the functional FP (Fig. 4).^{66,67} The first report of an RFP complementation system described one based on the Gln66Thr variant of mRFP1.⁶⁸ Later efforts used mCherry, mPlum, and mKate as the basis for FP complementation systems with longer emission wavelength and brighter fluorescence.^{69–71} Recently, an mNeptune-based complementation system was introduced and successfully applied for *in vivo* imaging of RNA–protein and protein–protein interactions.⁷²

All FP complementation systems are associated with some drawbacks and limitations, including background self-association and temperature sensitivity.⁷³ As FP complementation is effectively irreversible, it is useful for trapping both constitutive and transient protein–protein interactions. However, as formation of a mature chromophore in the reconstituted FP usually requires tens of minutes,^{71,74} FP complementation is unsuitable for dynamic visualization of reversible protein–protein interactions. Fortunately, the limitations imposed by the irreversibility and slow kinetics can be overcome using alternative biosensing strategies such as FRET or ddFPs.

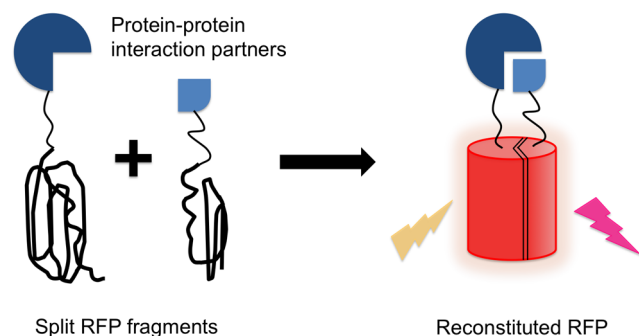


Fig. 4 Biosensor design based on RFP complementation. Two potentially interacting proteins are fused to the two fragments of a split RFP. Interaction between the two protein partners bring the RFP fragments in close proximity, leading to reconstitution of an intact RFP and a corresponding increase in red fluorescence.

2.3 RFP Biosensors Based on FRET

FRET is the phenomenon of radiationless energy transfer via dipole–dipole interaction between two chromophores that have compatible energy levels and are close in distance (<10 nm). The basic design principle of all FRET-based biosensors is to couple a specific binding event or covalent modification of a protein to a change of the energy transfer efficiency between the higher energy donor FP and the lower energy acceptor FP. A variety of FP FRET-based biosensors for detection of protein–protein interaction, ion concentrations, small molecule concentrations, and enzyme activities have been developed (Fig. 5).⁷⁵

The design of intermolecular FRET-based biosensors for protein–protein interaction detection is similar to that of FP complementation. However, rather than having the interacting proteins of interest fused to the FP fragments, they are fused to the donor FP and acceptor FP. FRET efficiency increases when the two protein partners interact to form a complex. For biosensor designs intended for detection of a protein conformational change, an intramolecular FRET-based biosensor can be constructed by linking both donor and acceptor FPs in a single polypeptide. The intramolecular biosensor design offers a more consistent signal output due to the fixed ratio of donor and acceptor concentrations in different cells.

The cyan and yellow FP-based FRET donor and receptor pair is an excellent choice for the construction of genetically encoded FRET biosensors due to the large spectral overlap and their relatively high brightness. However, the development of various monomeric RFP variants has now provided new and exciting possibilities to construct red-shifted FRET pairs. For example, mRuby2, currently one of the brightest monomeric RFPs, has been paired with a bright GFP variant, Clover.³⁶ This new FRET pair confers a greater dynamic range and photostability

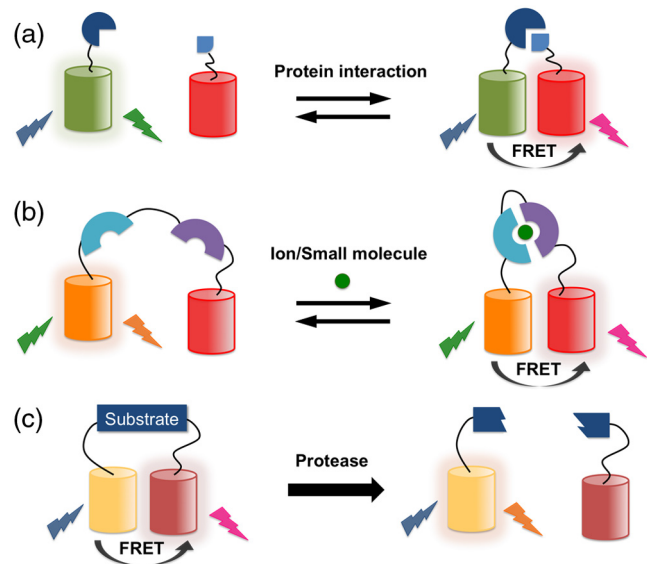


Fig. 5 Representative Förster resonance energy transfer (FRET)-based biosensors with RFPs. (a) Intermolecular biosensors for protein–protein interaction. Unlike FP complementation-based biosensors, the FRET-based biosensors of protein–protein interactions are reversible. (b) Ion/small molecule biosensors. An intramolecular protein complex is formed, or a conformation changed, upon the binding of a specific ion or small molecule. (c) Protease biosensors where the two FPs are initially linked by a protease substrate sequence.

compared to various existing cyan FP (CFP)- and yellow FP (YFP)-based FRET biosensors.

The availability of new RFPs also provides opportunities to construct new FRET pairs with novel spectral properties. One of the main justifications for such efforts is to achieve spectral compatibility with the CFP–YFP pair.^{76,77} For example, the mOrange–mCherry pair is spectrally orthogonal to the CFP–YFP pair, though FRET biosensors based on this pair tend to have only modest signal changes.^{78,79} The orange–red FRET pair was recently improved by developing self-associating variants of mOrange and mCherry by reversion of the hydrophobic dimeric interface breaking mutations.^{80,81} LSS mOrange and mKate2 are yet another orange–red FRET pair that has been simultaneously imaged with a CFP–YFP FRET pair using a single laser excitation wavelength.⁴⁷

Generally speaking, the single most important advantage of FRET-based biosensors is that they provide ratiometric fluorescent changes that can typically be calibrated, making this class of indicators most appropriate for quantitative imaging. The single major disadvantage of FRET-based biosensors is that the fluorescent changes are often quite small (as low as a few percent, though there are some with much larger changes).⁸² A second disadvantage is that FRET-based biosensors require two distinct emission channels for ratiometric imaging, making it challenging to use more than one type of biosensor in a single experiment.

2.4 RFP Biosensors Based on ddFPs

ddFPs are a relatively recent addition to the FP toolbox that provide an alternative platform for biosensor design.^{83,84} The ddFP strategy is based on a pair of FPs, engineered from dTomato, which exhibit minimal to no fluorescence in their monomeric states. Upon heterodimerization, the chromophore environment of one FP is modified such that the anionic state of the chromophore is stabilized, leading to an increase in red fluorescence. The first ddFP to be engineered was a red variant (ddRFP) with a 10-fold increase in red fluorescence intensity upon heterodimer formation. The dimerization-dependent fluorescence change of ddRFP was used for detection of reversible Ca^{2+} -dependent association of calmodulin (CaM) and M13 in live cells, as well as imaging of caspase-3 activity during apoptosis (Fig. 6).⁸⁴ Green and yellow ddFP pairs were later engineered and applied for detection of membrane–membrane contacts at the mitochondria associated membrane.⁸³

Although conceptually analogous to FP complementation, the advantage of ddFP lies in the reversibility of heterodimer formation. Accordingly, they can be used to visualize dynamic and reversible protein–protein interactions in live cells, similar to how FRET is used. Compared to FRET-based biosensors, ddFPs do have an inherent advantage for multiparameter imaging. Specifically, a ddFP occupies just one color channel (i.e., green, yellow, or red) while FRET-based biosensors occupies two (i.e., donor and acceptor). One drawback of ddFPs is that they will spontaneously dimerize at relatively high concentrations (above 10 μM). By contrast, FRET pairs have only a weak tendency to dimerize and the dissociation constants are typically much higher (>100 μM).⁸¹

2.5 RFP Biosensors Based on a Single FP

As their name implies, single FP-based biosensors contain only one engineered FP signal-transduction domain. The biosensor is

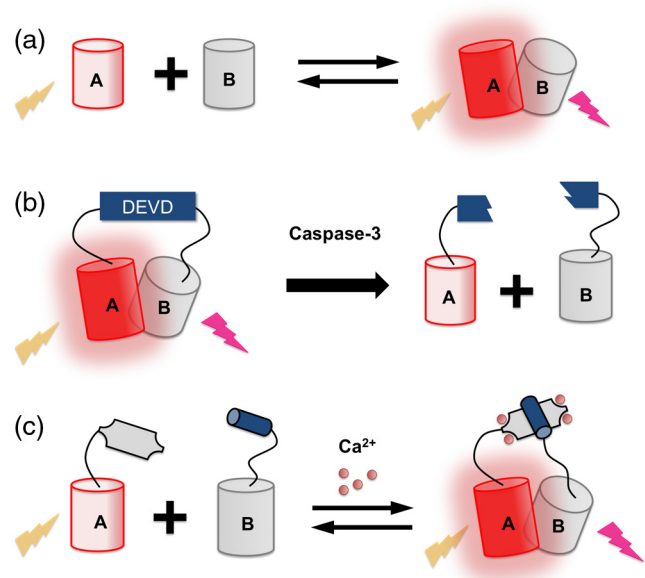


Fig. 6 ddRFPs and ddRFP-based biosensors. (a) Fluorescence intensity increase upon the formation of heterodimeric ddRFP pair. (b) ddRFP-based caspase-3 biosensor. (c) ddRFP-based Ca^{2+} biosensor.

engineered such that the FP responds to the biochemical stimulus of interest with a reversible change in fluorescence intensity (intensiometric), excitation spectral profile (excitation ratiometric), or emission spectral profile (emission ratiometric). The major advantage of single FP-based biosensors is that they typically exhibit a substantially larger intensity change at a single wavelength than a FRET-based biosensor. Furthermore, single FP-based biosensors have the benefit of using a smaller region of the visible spectrum window, enabling the simultaneous use of more than one fluorophore color. Yet another advantage relative to intramolecular FRET-based biosensors is the smaller protein size.

One way to create a single FP-based biosensor is to take advantage of the intrinsic sensitivities of certain FP variants [Fig. 7(a)]. For example, all FPs exhibit some pH dependence and some have apparent $\text{p}K_a$ s close to physiologically relevant pH values. Among the many examples of such FP-based pH biosensors, the most widely used are the pHlourin variants of avGFP.⁵⁶ The chloride ion sensitivity of YFP is another example of intrinsic FP sensitivity.^{85,86} It has also been proven possible to rationally engineer intrinsic sensitivity into an FP by incorporating an analyte binding site directly on the exterior of the FP barrel. For example, the reduction/oxidation sensitive roGFP^{87,88} and the calcium ion (Ca^{2+}) sensitive CatchER were engineered in this way.⁸⁹

The majority of intrinsic single FP-based biosensors are green or yellow fluorescent, and only a few intrinsic red single FP-based biosensors have been described. Examples include mNectarine, which was applied for detection of nucleoside transport,⁹⁰ and pHTomato, which was used to report synaptic neurotransmitter release at nerve terminals.⁵⁷ An excitation ratiometric pH biosensor, pHRed, was engineered from LSS RFP mKeima and used to image energy-dependent changes of cytosolic and mitochondrial pH.⁵⁸ Recently, a pH-sensitive RFP, known as pHuji, was engineered from mApple and used for imaging of endocytosis and exocytosis.⁵⁹

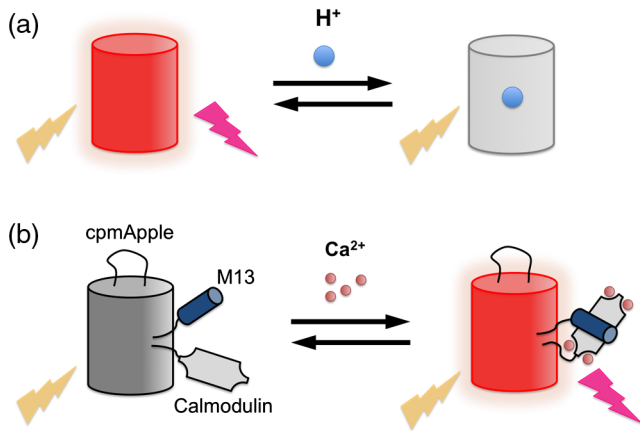


Fig. 7 Single FP-based biosensors. (a) Single FP-based pH biosensor based on intrinsic sensitivity. (b) Single FP-based Ca^{2+} biosensor with an extrinsic Ca^{2+} binding domain.

Another strategy for engineering a single FP-based biosensor is to genetically incorporate an extrinsic analyte recognition domain into the FP. The extrinsic domain is typically fused to one of the termini or inserted into a solvent-exposed region of the FP in order to minimize disruption of the protein structure. For the FP to work as an effective signal transducer, the extrinsic recognition domain must be in relatively close proximity to the chromophore to allosterically modulate the chromophore environment upon interaction with the target analyte. It is important to note that the FP chromophore is well protected in the center of the barrel structure, and the termini and loop region are relatively distant from the chromophore. An extrinsic recognition domain fused to one of the termini is unlikely to have much influence on the chromophore environment. To circumvent this problem, researchers rely on the strategy of circular permutation (Fig. 8). Circularly permuted FPs are generated by genetically linking the original N- and C-termini with a short polypeptide linker and introducing new N- and C-termini at a position elsewhere in the protein.^{91,92} For FP-based biosensor construction, the new N- and C-termini are introduced close to the chromophore such that conformational changes in the extrinsic recognition element cause alterations in the chromophore environment and, correspondingly, in the fluorescence intensity or hue of the FP.⁹³⁻⁹⁶

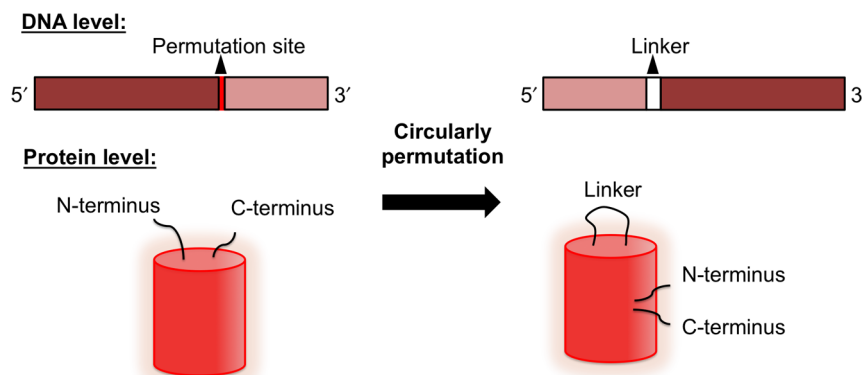


Fig. 8 Schematic presentation of FP circular permutation at both the DNA and protein levels.

3 Emerging Toolset for Neurophotonics Based on RFPs

An increasing number of RFP-based probes are being applied in neurophotonics applications. Representative applications include tagging of specific neuron subsets,⁹⁷ visualizing membrane depolarization,⁹⁸ and monitoring ion concentration dynamics of downstream signaling cascades.⁹⁹ Importantly, RFP-based neural activity biosensors offer the possibility of combining with blue-light activated optogenetic actuators, such as channelrhodopsin-2 (ChR2), for simultaneous stimulation and read-out of neuronal activities.

3.1 RFP-Based Ca^{2+} Biosensors

Ca^{2+} is the principal secondary messenger associated with neuronal signaling pathways and is reliably elevated during the firing of action potentials. Accordingly, FP-based Ca^{2+} biosensors are exceptionally useful for the imaging of neuronal activity in contexts ranging from *in vitro* cultured cells to *in vivo* brain activity in behaving animals.

Over the last decade, the GCaMP-type single FP-based biosensors have emerged as the predominant technology for *in vivo* imaging of neuronal activity.^{100,101} GCaMP is composed of cpGFP with M13 and CaM fused to the N- and C- termini, respectively. Structural studies reveal that in its Ca^{2+} free state, the fluorescence is quenched because the chromophore is exposed to bulk solvent. In the presence of Ca^{2+} , CaM wraps around M13 and forms a new interaction with the chromophore that stabilizes the phenolate (i.e., the fluorescent form) state.

Following the GCaMP-type design strategy, a red Ca^{2+} biosensor known as R-GECO1⁶⁰ was created by replacing the cpGFP in an improved GCaMP variant with a circularly permuted variant of mApple. R-GECO1 was further optimized and engineered into spectrally diversified and low-affinity variants, including an improved R-GECO1.2, a blue-shifted O-GECO, a red-shifted CAR-GECO,¹⁰² a highlightable GR-GECO,¹⁰³ an LSS REX-GECO¹⁰⁴ and low-affinity red-GECO variants.¹⁰⁵ RCaMP, a similar single RFP-based Ca^{2+} biosensor, was engineered from the cpmRuby template.¹⁰⁶ Further improved variants of R-GECO1, confusingly named R-CaMP1.07 and R-CaMP2, have recently been reported.^{107,108}

The development of mApple-based R-GECO1⁶⁰ and mRuby-based RCaMP,¹⁰⁶ has unlocked new opportunities for simultaneous multicolor optical imaging for neural activities as well as

integration of optogenetics for orthogonal activation and measurement. For example, R-GECO1 has been used to report neural activity *in vivo* in the zebrafish retinotectal system, with comparable performance to the green Ca^{2+} biosensor GCaMP3.¹⁰⁹ CAR-GECO1, a red-shifted variant based on R-GECO1, was used for optogenetic activation and Ca^{2+} imaging concurrently in combination with channelrhodopsin-2(T159C)-EGFP in mouse neocortical slice culture.¹⁰² RCaMP, along with green glutamate sensor, was used for imaging synaptic input and output in *Caenorhabditis elegans* neurons.⁹³ The LSS REX-GECO1 was used in the eye and optic tectum of albino *Xenopus laevis* tadpoles for two-photon fluorescence imaging of Ca^{2+} dynamics *in vivo*.¹⁰⁴

Due to an inherent tendency of mApple to undergo photoactivation (i.e., a temporary increase in brightness that can be easily confused with a true Ca^{2+} elevation) with blue light, one must be cautious when using R-GECO series indicators with optogenetic tools requiring violet/blue activation light.¹⁰² In comparison, this photoactivation effect was not observed from mRuby-based RCaMP series indicators. Therefore, RCaMP should be a better-suited Ca^{2+} indicator for use with ChR2 or other violet/blue light activatable optogenetic tools.

3.2 RFP-Based Voltage Biosensors

For imaging of neuronal activity, the signals obtained from an FP-based Ca^{2+} biosensor are, necessarily, only a surrogate for action potentials. Nevertheless, this indirect measure has proven to be very useful, largely because Ca^{2+} biosensors have traditionally been far superior to voltage biosensors in terms of their brightness and magnitude of fluorescence response. The trade-offs associated with the reliance on Ca^{2+} signals (which have much slower temporal dynamics than voltage changes) are that neither fast series of spiking events, nor subthreshold voltage changes, can be visualized. In order to overcome these limitations, biosensors that directly report on membrane voltage are needed.¹¹⁰ Accordingly, the FP research community has been pursuing the development of voltage indicators for as long as they have been pursuing FP-based Ca^{2+} biosensors, though with more modest success to date.

Both FRET-based and single FP-based voltage sensors for imaging of membrane potential changes in neurons have been reported. These indicators are constructed by tethering an FP, or a FRET pair of FPs, to a voltage-sensitive membrane protein, such that a voltage-dependent conformation change alters either the brightness of the FP or the FRET efficiency, respectively. Some notable examples include FlaSh/Flare,^{111,112} SPARC,¹¹³ and the voltage-sensitive FPs.^{110,114,115} These indicators have undergone improvements resulting in variants with faster kinetics,¹¹⁶ improved cell surface targeting,¹¹⁷ and larger signal changes.¹¹³ Despite these improvements, voltage indicators have been notoriously challenging to apply in research applications, especially when judged against highly optimized and robust GCaMP-type Ca^{2+} indicators. One of the most pressing issues with FP-based voltage sensors was their relatively small signal changes, with all sensors reported prior to 2012 exhibiting maximal fluorescence changes of <10%.^{118,119}

In 2012, Jin et al.¹²⁰ reported a GFP-based voltage biosensor, Arclight, with an unprecedented 35% decrease in fluorescence intensity in response to a 100 mV depolarization. Arclight provides sufficient brightness and signal change to enable detection of single action potentials and subthreshold activities in individual neurons and dendrites, although with relatively slow

response kinetics. Further engineered Arclight variants provided faster kinetics but at the expense of reduced signal changes.¹²¹ Accelerated sensor of action potentials 1 (ASAP1) is another recently developed green fluorescent voltage sensor.⁹⁵ As its name implies, it offers faster kinetics relative to Arclight and enables continuous monitoring of membrane potential in neurons at kilohertz frame rates using standard epifluorescence microscopy.

Efforts to develop red fluorescent voltage indicators have lagged behind the efforts to develop green ones. VSFP_cpmKate, VSFP3.1_TagRFP, and VSFP3.1_mKate2 are some examples of voltage indicators that emit in the red region of the visible spectrum.^{122,123} However, the fluorescence brightness, response amplitude, and kinetics of these red-shifted VSFPs are not comparable to that of Arclight or ASAP1. In unpublished work, our group has developed a red fluorescent voltage biosensor, designated FlicR1, which is based on the voltage-sensing domain of Arclight and the cpmApple of R-GECO1 (Ahmed Abdelfattah, unpublished results).

3.3 RFP-Based Synaptic Transmission Biosensors

Yet another important application of FP-based biosensors is the detection of synaptic transmission. The first FP designed for the purpose of detecting vesicle fusion at the synapse was synapto-pHluorin.^{56,124} To engineer synapto-pHluorin, a pH-sensitive variant of avGFP, known as superecliptic pHluorin (SEP),¹²⁵ was fused to the luminal side of the vesicular protein, synapto-brevin. SEP is initially quenched by the acidic conditions of the vesicle lumen but increases in fluorescence ~20-fold upon release of the vesicle contents following fusion with the plasma membrane. Fusing SEP to proteins highly localized to synaptic vesicles, such as synaptophysin¹²⁶ or the glutamate transporter VGLut1,¹²⁷ resulted in improved signal-to-noise ratios.

As with other classes of biosensors, efforts to develop an RFP-based biosensor of synaptic fusion lagged far behind the development of the GFP-based biosensor. By taking advantage of the pH-sensitive property of the orange FP mOrange2, a red-shifted biosensor was constructed by fusion to VGLut1.¹²⁸ Designated as VGLut1-mOrange2, this probe was used in conjunction with GCaMP3 to simultaneously image synaptic vesicle recycling and changes in cytosolic Ca^{2+} . In a similar application, the pH-sensitive pHTomato RFP was coexpressed with GCaMP3 for concomitant imaging of neurotransmitter release and presynaptic Ca^{2+} transients at single nerve terminals.⁵⁷ Coexpression of pHTomato and ChR2 provided an all-optical approach for multiplex control and tracking of distinct circuit pathways.

Another approach to visualizing synaptic transmission is to detect the neurotransmitter itself. For example, the genetically encoded biosensor GluSnFR is a FRET-based biosensor that incorporates the periplasmic glutamate-binding protein GltI as a molecular recognition element.¹²⁹ A single FP-based green glutamate biosensor called iGluSnFR was also engineered by insertion of a cpGFP into the glutamate-binding domain GltI.⁹³ In unpublished work, our group has converted iGluSnFR⁹³ into a red fluorescent variant by substituting the cpGFP with the cpmApple domain from R-GECO1 (Jiahui Wu, unpublished results).

4 Conclusion and Outlook

Since the advent of DsRed and its subsequent monomerization, the number of useful RFP variants and RFP-based biosensors

has continued to grow steadily. These enhanced RFPs and RFP-based biosensors have brought new color options to the existing FP spectrum and provided new possibilities for multiparameter investigations of biological problems. Unfortunately, despite the great strides that have been made, few of the RFPs and RFP-based biosensors come close to matching their green fluorescent counterparts in terms of utility for neuroscience research.

Both anecdotally and in published reports, many RFP and RFP-based biosensors have been reported to perform suboptimally in transfected neural tissues or transgenic animals.⁹⁷ While this is disappointing, one important factor to keep in mind is that optimization of some of the most effective GFP-based biosensors (e.g., GCaMP) has been ongoing for more than a decade. In comparison, practically all of the RFP-based biosensors reviewed here were reported within the past 4 years and are early-generation versions that will surely improve with future optimization. One of the problems most commonly encountered with RFPs is their unexpectedly dim fluorescence and protein mislocalization or accumulation, often manifested as bright puncta in the soma. Mounting evidence attributes these bright puncta to accumulation of RFPs in lysosomes or autophagosomes.^{50,51} RFPs can also suffer from reversible conversion to a transient dark state.^{130,131}

Protein engineers continue to work on creating ever-better RFPs, yet, to date, an RFP that matches the best avGFP variants in all performance characteristics remains elusive. Nevertheless, we remain confident that such an RFP, or far RFP, will be engineered in the near future. In addition, we expect that with further efforts and advanced screening techniques,¹³² the performance of RFP-based biosensors will catch up to and eventually exceed their green counterparts. Ultimately, we expect that the inherent benefits associated with longer wavelength fluorescence will allow RFPs to surpass GFPs as the default fluorophores for live cell imaging and neurophotonic applications.

Acknowledgments

We thank the Natural Sciences and Engineering Research Council of Canada, the Canadian Institutes of Health Research, the Alberta Glycomics Centre, the University of Alberta (Queen Elizabeth II scholarship to T.L.), and Alberta Innovates (scholarship to Y.S.) for funding support.

References

- O. Shimomura, F. H. Johnson, and Y. Saiga, "Extraction, purification and properties of aequorin, a bioluminescent protein from the luminous hydromedusa, *Aequorea*," *J. Cell. Comp. Physiol.* **59**(3), 223–239 (1962).
- O. Shimomura, "Structure of the chromophore of *Aequorea* green fluorescent protein," *FEBS Lett.* **104**(2), 220–222 (1979).
- D. C. Prasher et al., "Primary structure of the *Aequorea victoria* green-fluorescent protein," *Gene* **111**(2), 229–233 (1992).
- M. Chalfie et al., "Green fluorescent protein as a marker for gene-expression," *Science* **263**(5148), 802–805 (1994).
- R. Heim, D. C. Prasher, and R. Y. Tsien, "Wavelength mutations and posttranslational autooxidation of green fluorescent protein," *Proc. Natl. Acad. Sci. U. S. A.* **91**(26), 12501–12504 (1994).
- R. Heim, A. B. Cubitt, and R. Y. Tsien, "Improved green fluorescence," *Nature* **373**(6516), 663–664 (1995).
- R. Heim and R. Y. Tsien, "Engineering green fluorescent protein for improved brightness, longer wavelengths and fluorescence resonance energy transfer," *Curr. Biol.* **6**(2), 178–182 (1996).
- T. T. Yang, L. Cheng, and S. R. Kain, "Optimized codon usage and chromophore mutations provide enhanced sensitivity with the green fluorescent protein," *Nucleic Acids Res.* **24**(22), 4592–4593 (1996).
- A. S. Mishin et al., "The first mutant of the *Aequorea victoria* green fluorescent protein that forms a red chromophore," *Biochemistry* **47**(16), 4666–4673 (2008).
- M. V. Matz et al., "Fluorescent proteins from nonbioluminescent Anthozoa species," *Nat. Biotechnol.* **17**(10), 969–973 (1999).
- G. S. Baird, D. A. Zacharias, and R. Y. Tsien, "Biochemistry, mutagenesis, and oligomerization of DsRed, a red fluorescent protein from coral," *Proc. Natl. Acad. Sci. U. S. A.* **97**(22), 11984–11989 (2000).
- M. Cotlet et al., "Identification of different emitting species in the red fluorescent protein DsRed by means of ensemble and single-molecule spectroscopy," *Proc. Natl. Acad. Sci. U. S. A.* **98**(25), 1439–14403 (2001).
- L. A. Gross et al., "The structure of the chromophore within DsRed, a red fluorescent protein from coral," *Proc. Natl. Acad. Sci. U. S. A.* **97**(22), 11990–11995 (2000).
- D. Yarbrough et al., "Refined crystal structure of DsRed, a red fluorescent protein from coral, at 2.0-Å resolution," *Proc. Natl. Acad. Sci. U. S. A.* **98**(2), 462–467 (2001).
- R. E. Campbell et al., "A monomeric red fluorescent protein," *Proc. Natl. Acad. Sci. U. S. A.* **99**(12), 7877–7882 (2002).
- N. C. Shaner et al., "Improved monomeric red, orange and yellow fluorescent proteins derived from *Discosoma* sp. red fluorescent protein," *Nat. Biotechnol.* **22**(12), 1567–1572 (2004).
- N. C. Shaner et al., "Improving the photostability of bright monomeric orange and red fluorescent proteins," *Nat. Methods* **5**(6), 545–551 (2008).
- X. Shu et al., "Novel chromophores and buried charges control color in mFruits," *Biochemistry* **45**(32), 9639–9647 (2006).
- S. Pletnev et al., "A crystallographic study of bright far-red fluorescent protein mKate reveals pH-induced cis-trans isomerization of the chromophore," *J. Biol. Chem.* **283**(43), 28980–28987 (2008).
- M. Ormo et al., "Crystal structure of the *Aequorea victoria* green fluorescent protein," *Science* **273**(5280), 1392–1395 (1996).
- V. V. Verkhusha et al., "Common pathway for the red chromophore formation in fluorescent proteins and chromoproteins," *Chem. Biol.* **11**(6), 845–854 (2004).
- R. N. Day and M. W. Davidson, "The fluorescent protein palette: tools for cellular imaging," *Chem. Soc. Rev.* **38**(10), 2887–2921 (2009).
- R. L. Strack et al., "Chromophore formation in DsRed occurs by a branched pathway," *J. Am. Chem. Soc.* **132**(24), 8496–8505 (2010).
- F. V. Subach and V. V. Verkhusha, "Chromophore transformations in red fluorescent proteins," *Chem. Rev.* **112**(7), 4308–4327 (2012).
- W. Tomosugi et al., "An ultramarine fluorescent protein with increased photostability and pH insensitivity," *Nat. Methods* **6**(5), 351–353 (2009).
- N. C. Shaner, P. A. Steinbach, and R. Y. Tsien, "A guide to choosing fluorescent proteins," *Nat. Methods* **2**(12), 905–909 (2005).
- N. C. Shaner, G. H. Patterson, and M. W. Davidson, "Advances in fluorescent protein technology," *J. Cell Sci.* **120**(24), 4247–4260 (2007).
- M. Z. Lin et al., "Autofluorescent proteins with excitation in the optical window for intravital imaging in mammals," *Chem. Biol.* **16**(11), 1169–1179 (2009).
- F. V. Subach et al., "Photoactivatable mCherry for high-resolution two-color fluorescence microscopy," *Nat. Methods* **6**(2), 153–159 (2009).
- A. C. Stiel et al., "Generation of monomeric reversibly switchable red fluorescent proteins for far-field fluorescence nanoscopy," *Biophys. J.* **95**(6), 2989–2997 (2008).
- F. V. Subach et al., "Red fluorescent protein with reversibly photo-switchable absorbance for photochromic FRET," *Chem. Biol.* **17**(7), 745–755 (2010).
- O. M. Subach et al., "A photoswitchable orange-to-far-red fluorescent protein, PSmOrange," *Nat. Methods* **8**, 771–777 (2011).
- V. Adam et al., "Phototransformable fluorescent proteins: Future challenges," *Curr. Opin. Chem. Biol.* **20**, 92–102 (2014).
- E. M. Merzlyak et al., "Bright monomeric red fluorescent protein with an extended fluorescence lifetime," *Nat. Methods* **4**(7), 555–557 (2007).
- S. Kredel et al., "mRuby, a bright monomeric red fluorescent protein for labeling of subcellular structures," *PLoS One* **4**(2), e4391 (2009).
- A. J. Lam et al., "Improving FRET dynamic range with bright green and red fluorescent proteins," *Nat. Methods* **9**(10), 1005–1012 (2012).
- I. Shemiakina et al., "A monomeric red fluorescent protein with low cytotoxicity," *Nat. Commun.* **3**, 1204 (2012).

38. D. Shcherbo et al., "Bright far-red fluorescent protein for whole-body imaging," *Nat. Methods* **4**(9), 741–746 (2007).
39. D. Shcherbo et al., "Far-red fluorescent tags for protein imaging in living tissues," *Biochem. J.* **418**(3), 567–574 (2009).
40. L. Wang et al., "Evolution of new nonantibody proteins via iterative somatic hypermutation," *Proc. Natl. Acad. Sci. U. S. A.* **101**(48), 16745–16749 (2004).
41. K. S. Morozova et al., "Far-red fluorescent protein excitable with red lasers for flow cytometry and superresolution STED nanoscopy," *Biophys. J.* **99**(2), L13–15 (2010).
42. K. D. Piatkevich et al., "Extended Stokes shift in fluorescent proteins: chromophore-protein interactions in a near-infrared TagRFP675 variant," *Sci. Rep.* **3**, 1847 (2013).
43. J. Chu et al., "Non-invasive intravital imaging of cellular differentiation with a bright red-excitable fluorescent protein," *Nat. Methods* **11**(5), 572–578 (2014).
44. T. Kogure et al., "A fluorescent variant of a protein from the stony coral *Montipora* facilitates dual-color single-laser fluorescence cross-correlation spectroscopy," *Nat. Biotechnol.* **24**(5), 577–581 (2006).
45. J. Yang et al., "mBeRFP, an improved large Stokes shift red fluorescent protein," *PLoS One* **8**(6), e64849 (2013).
46. K. D. Piatkevich et al., "Monomeric red fluorescent proteins with a large Stokes shift," *Proc. Natl. Acad. Sci. U. S. A.* **107**(12), 5369–5374 (2010).
47. D. M. Shcherbakova et al., "An orange fluorescent protein with a large Stokes shift for single-excitation multicolor FCCS and FRET imaging," *J. Am. Chem. Soc.* **134**(18), 7913–7923 (2012).
48. J. Wiedenmann et al., "A far-red fluorescent protein with fast maturation and reduced oligomerization tendency from *Entacmaea quadricolor* (Anthozoa, Actinaria)," *Proc. Natl. Acad. Sci. U. S. A.* **99**(18), 11646–11651 (2002).
49. L. M. Costantini et al., "Assessing the tendency of fluorescent proteins to oligomerize under physiologic conditions," *Traffic* **13**(5), 643–649 (2012).
50. H. Katayama et al., "GFP-like proteins stably accumulate in lysosomes," *Cell Struct. Funct.* **33**(1), 1–12 (2008).
51. S. Maday, K. E. Wallace, and E. L. Holzbaur, "Autophagosomes initiate distally and mature during transport toward the cell soma in primary neurons," *J. Cell Biol.* **196**(4), 407–417 (2012).
52. R. A. Chica et al., "Generation of longer emission wavelength red fluorescent proteins using computationally designed libraries," *Proc. Natl. Acad. Sci. U. S. A.* **107**(47), 20257–20262 (2010).
53. K. D. Piatkevich et al., "Engineering ESPT pathways based on structural analysis of LSSmKate red fluorescent proteins with large Stokes shift," *J. Am. Chem. Soc.* **132**(31), 10762–10770 (2010).
54. J. Zhang et al., "Creating new fluorescent probes for cell biology," *Nat. Rev. Mol. Cell Biol.* **3**(12), 906–918 (2002).
55. B. Wu et al., "Modern fluorescent proteins and imaging technologies to study gene expression, nuclear localization, and dynamics," *Curr. Opin. Cell Biol.* **23**(3), 310–317 (2011).
56. G. Miesenböck, D. A. De Angelis, and J. E. Rothman, "Visualizing secretion and synaptic transmission with pH-sensitive green fluorescent proteins," *Nature* **394**(6689), 192–195 (1998).
57. Y. Li and R. W. Tsien, "pHTomato, a red, genetically encoded indicator that enables multiplex interrogation of synaptic activity," *Nat. Neurosci.* **15**(7), 1047–1053 (2012).
58. M. Tantama, Y. P. Hung, and G. Yellen, "Imaging intracellular pH in live cells with a genetically encoded red fluorescent protein sensor," *J. Am. Chem. Soc.* **133**(26), 10034–10037 (2011).
59. Y. Shen et al., "pHuji, a pH-sensitive red fluorescent protein for imaging of exo- and endocytosis," *J. Cell Biol.* **207**(3), 419–432 (2014).
60. Y. Zhao et al., "An expanded palette of genetically encoded Ca²⁺(+) indicators," *Science* **333**(6051), 1888–1891 (2011).
61. J. Berg, Y. P. Hung, and G. Yellen, "A genetically encoded fluorescent reporter of ATP:ADP ratio," *Nat. Methods* **6**(2), 161–166 (2009).
62. M. B. Cannon and S. J. Remington, "Re-engineering redox-sensitive green fluorescent protein for improved response rate," *Protein Sci.* **15**(1), 45–57 (2006).
63. D. Dimitrov et al., "Engineering and characterization of an enhanced fluorescent protein voltage sensor," *PLoS One* **2**(5), e440 (2007).
64. T. Yano et al., "A novel fluorescent sensor protein for visualization of redox states in the cytoplasm and in peroxisomes," *Mol. Cell Biol.* **30**(15), 3758–3766 (2010).
65. R. H. Newman, M. D. Fosbrink, and J. Zhang, "Genetically encodable fluorescent biosensors for tracking signaling dynamics in living cells," *Chem. Rev.* **111**(5), 3614–3666 (2011).
66. I. Ghosh, A. D. Hamilton, and L. Regan, "Antiparallel leucine zipper-directed protein reassembly: application to the green fluorescent protein," *J. Am. Chem. Soc.* **122**(23), 5658–5659 (2000).
67. C. G. Wilson, T. J. Magliery, and L. Regan, "Detecting protein-protein interactions with GFP-fragment reassembly," *Nat. Methods* **1**(3), 255–262 (2004).
68. G. Jach et al., "An improved mRFP1 adds red to bimolecular fluorescence complementation," *Nat. Methods* **3**(8), 597–600 (2006).
69. J. Y. Fan et al., "Split mCherry as a new red bimolecular fluorescence complementation system for visualizing protein-protein interactions in living cells," *Biochem. Biophys. Res. Commun.* **367**(1), 47–53 (2008).
70. J. O. Keem et al., "Splitting and self-assembling of far-red fluorescent protein with an engineered beta strand peptide: application for alpha-synuclein imaging in mammalian cells," *Biomaterials* **32**(34), 9051–9058 (2011).
71. J. Chu et al., "A novel far-red bimolecular fluorescence complementation system that allows for efficient visualization of protein interactions under physiological conditions," *Biosens. Bioelectron.* **25**(1), 234–239 (2009).
72. Y. Han et al., "In vivo imaging of protein-protein and RNA-protein interactions using novel far-red fluorescence complementation systems," *Nucleic Acids Res.* **42**(13), e103 (2014).
73. G. S. Filonov and V. V. Verkhusha, "A near-infrared BiFC reporter for in vivo imaging of protein-protein interactions," *Chem. Biol.* **20**(8), 1078–1086 (2013).
74. S. Cabantous et al., "A new protein-protein interaction sensor based on tripartite split-GFP association," *Sci. Rep.* **3**, 2854 (2013).
75. L. Lindenburg and M. Merckx, "Engineering genetically encoded FRET sensors," *Sensors* **14**(7), 11691–11713 (2014).
76. H. W. Ai et al., "Fluorescent protein FRET pairs for ratiometric imaging of dual biosensors," *Nat. Methods* **5**(5), 401–403 (2008).
77. H. J. Carlson and R. E. Campbell, "Genetically encoded FRET-based biosensors for multiparameter fluorescence imaging," *Curr. Opin. Biotechnol.* **20**(1), 19–27 (2009).
78. J. Goedhart et al., "Sensitive detection of p65 homodimers using red-shifted and fluorescent protein-based FRET couples," *PLoS One* **2**(10), e1011 (2007).
79. A. Piljic and C. Schultz, "Simultaneous recording of multiple cellular events by FRET," *ACS Chem. Biol.* **3**(3), 156–160 (2008).
80. L. H. Lindenburg et al., "Robust red FRET sensors using self-associating fluorescent domains," *ACS Chem. Biol.* **8**(10), 2133–2139 (2013).
81. L. H. Lindenburg et al., "Quantifying stickiness: thermodynamic characterization of intramolecular domain interactions to guide the design of Förster resonance energy transfer sensors," *Biochemistry* **53**(40), 6370–6381 (2014).
82. R. E. Campbell, "Fluorescent-protein-based biosensors: modulation of energy transfer as a design principle," *Anal. Chem.* **81**(15), 5972–5979 (2009).
83. S. C. Alford et al., "Dimerization-dependent green and yellow fluorescent proteins," *ACS Synth. Biol.* **1**(12), 569–575 (2012).
84. S. C. Alford et al., "A fluorogenic red fluorescent protein heterodimer," *Chem. Biol.* **19**(3), 353–360 (2012).
85. S. Jayaraman et al., "Mechanism and cellular applications of a green fluorescent protein-based halide sensor," *J. Biol. Chem.* **275**(9), 6047–6050 (2000).
86. L. J. Galletta, P. M. Haggie, and A. S. Verkman, "Green fluorescent protein-based halide indicators with improved chloride and iodide affinities," *FEBS Lett.* **499**(3), 220–224 (2001).
87. G. T. Hanson et al., "Investigating mitochondrial redox potential with redox-sensitive green fluorescent protein indicators," *J. Biol. Chem.* **279**(13), 13044–13053 (2004).
88. C. T. Dooley et al., "Imaging dynamic redox changes in mammalian cells with green fluorescent protein indicators," *J. Biol. Chem.* **279**(21), 22284–22293 (2004).
89. S. Tang et al., "Design and application of a class of sensors to monitor Ca²⁺ dynamics in high Ca²⁺ concentration cellular compartments," *Proc. Natl. Acad. Sci. U. S. A.* **108**(39), 16265–16270 (2011).
90. D. E. Johnson et al., "Red fluorescent protein pH biosensor to detect concentrative nucleoside transport," *J. Biol. Chem.* **284**(31), 20499–20511 (2009).

91. H. J. Carlson, D. W. Cotton, and R. E. Campbell, "Circularly permuted monomeric red fluorescent proteins with new termini in the beta-sheet," *Protein Sci.* **19**(8), 1490–1499 (2010).
92. B. Shui et al., "Circular permutation of red fluorescent proteins," *PLoS One* **6**(5), e20505 (2011).
93. J. S. Marvin et al., "An optimized fluorescent probe for visualizing glutamate neurotransmission," *Nat. Methods* **10**(2), 162–170 (2013).
94. M. Tantama et al., "Imaging energy status in live cells with a fluorescent biosensor of the intracellular ATP-to-ADP ratio," *Nat. Commun.* **4**, 2550 (2013).
95. F. St-Pierre et al., "High-fidelity optical reporting of neuronal electrical activity with an ultrafast fluorescent voltage sensor," *Nat. Neurosci.* **17**(6), 884–889 (2014).
96. J. S. Marvin et al., "A genetically encoded, high-signal-to-noise maltose sensor," *Proteins* **79**(11), 3025–3036 (2011).
97. D. Cai et al., "Improved tools for the Brainbow toolbox," *Nat. Methods* **10**(6), 540–547 (2013).
98. H. Mutoh et al., "Optogenetic monitoring of membrane potentials," *Exp. Physiol.* **96**(1), 13–18 (2011).
99. S. Su et al., "Genetically encoded calcium indicator illuminates calcium dynamics in primary cilia," *Nat. Methods* **10**(11), 1105–1107 (2013).
100. J. Nakai, M. Ohkura, and K. Imoto, "A high signal-to-noise Ca²⁺ probe composed of a single green fluorescent protein," *Nat. Biotechnol.* **19**(2), 137–141 (2001).
101. T. Nagai et al., "Circularly permuted green fluorescent proteins engineered to sense Ca²⁺," *Proc. Natl. Acad. Sci. U. S. A.* **98**(6), 3197–3202 (2001).
102. J. Wu et al., "Improved orange and red Ca(2)+/- indicators and photo-physical considerations for optogenetic applications," *ACS Chem. Neurosci.* **4**(6), 963–972 (2013).
103. H. Hoi et al., "Highlightable Ca²⁺ indicators for live cell imaging," *J. Am. Chem. Soc.* **135**(1), 46–49 (2013).
104. J. Wu et al., "A long Stokes shift red fluorescent Ca(2+) indicator protein for two-photon and ratiometric imaging," *Nat. Commun.* **5**, 5262 (2014).
105. J. Wu et al., "Red fluorescent genetically encoded Ca²⁺ indicators for use in mitochondria and endoplasmic reticulum," *Biochem. J.* **464**(1), 13–22 (2014).
106. J. Akerboom et al., "Genetically encoded calcium indicators for multi-color neural activity imaging and combination with optogenetics," *Front. Mol. Neurosci.* **6**, 2 (2013).
107. M. Ohkura et al., "An improved genetically encoded red fluorescent Ca²⁺ indicator for detecting optically evoked action potentials," *PLoS One* **7**(7), e39933 (2012).
108. M. Inoue et al., "Rational design of a high-affinity, fast, red calcium indicator R-CaMP2," *Nat. Methods* **12**(1), 64–70 (2015).
109. A. S. Walker, J. Burrone, and M. P. Meyer, "Functional imaging in the zebrafish retinotectal system using RGECO," *Front. Neural Circuits* **7**, 34 (2013).
110. A. Perron et al., "Second and third generation voltage-sensitive fluorescent proteins for monitoring membrane potential," *Front. Mol. Neurosci.* **2**, 5 (2009).
111. M. S. Siegel and E. Y. Isacoff, "A genetically encoded optical probe of membrane voltage," *Neuron* **19**(4), 735–741 (1997).
112. B. J. Baker et al., "Three fluorescent protein voltage sensors exhibit low plasma membrane expression in mammalian cells," *J. Neurosci. Methods* **161**(1), 32–38 (2007).
113. K. Ataka and V. A. Pieribone, "A genetically targetable fluorescent probe of channel gating with rapid kinetics," *Biophys. J.* **82**(1), 509–516 (2002).
114. R. Sakai et al., "Design and characterization of a DNA-encoded, voltage-sensitive fluorescent protein," *Eur. J. Neurosci.* **13**(12), 2314–2318 (2001).
115. A. Lundby et al., "Engineering of a genetically encodable fluorescent voltage sensor exploiting fast Ci-VSP voltage-sensing movements," *PLoS One* **3**(6), e2514 (2008).
116. G. Guerrero et al., "Tuning FlaSh: redesign of the dynamics, voltage range, and color of the genetically encoded optical sensor of membrane potential," *Biophys. J.* **83**(6), 3607–3618 (2002).
117. L. Jin et al., "Random insertion of split-cans of the fluorescent protein venus into Shaker channels yields voltage sensitive probes with improved membrane localization in mammalian cells," *J. Neurosci. Methods* **199**(1), 1–9 (2011).
118. J. M. Kralj et al., "Electrical spiking in Escherichia coli probed with a fluorescent voltage-indicating protein," *Science* **333**(6040), 345–348 (2011).
119. L. Sjulson and G. Miesenbock, "Optical recording of action potentials and other discrete physiological events: a perspective from signal detection theory," *Physiology (Bethesda)* **22**, 47–55 (2007).
120. L. Jin et al., "Single action potentials and subthreshold electrical events imaged in neurons with a fluorescent protein voltage probe," *Neuron* **75**(5), 779–785 (2012).
121. Z. Han et al., "Fluorescent protein voltage probes derived from ArcLight that respond to membrane voltage changes with fast kinetics," *PLoS One* **8**(11), e81295 (2013).
122. S. G. Gautam et al., "Exploration of fluorescent protein voltage probes based on circularly permuted fluorescent proteins," *Front. Neuroeng.* **2**, 14 (2009).
123. A. Perron et al., "Red-shifted voltage-sensitive fluorescent proteins," *Chem. Biol.* **16**(12), 1268–1277 (2009).
124. G. Miesenbock, "Synapto-pHluorins: genetically encoded reporters of synaptic transmission," *Cold Spring Harb. Protoc.* **2012**(2), 213–217 (2012).
125. S. Sankaranarayanan et al., "The use of pHluorins for optical measurements of presynaptic activity," *Biophys. J.* **79**(4), 2199–2208 (2000).
126. Y. Zhu, J. Xu, and S. F. Heinemann, "Two pathways of synaptic vesicle retrieval revealed by single-vesicle imaging," *Neuron* **61**(3), 397–411 (2009).
127. J. Balaji and T. A. Ryan, "Single-vesicle imaging reveals that synaptic vesicle exocytosis and endocytosis are coupled by a single stochastic mode," *Proc. Natl. Acad. Sci. U. S. A.* **104**(51), 20576–20581 (2007).
128. H. Li et al., "Concurrent imaging of synaptic vesicle recycling and calcium dynamics," *Front. Mol. Neurosci.* **4**, 34 (2011).
129. S. A. Hires, Y. Zhu, and R. Y. Tsien, "Optical measurement of synaptic glutamate spillover and reuptake by linker optimized glutamate-sensitive fluorescent reporters," *Proc. Natl. Acad. Sci. U. S. A.* **105**(11), 4411–4416 (2008).
130. A. P. Siegel et al., "Strengths and weaknesses of recently engineered red fluorescent proteins evaluated in live cells using fluorescence correlation spectroscopy," *Int. J. Mol. Sci.* **14**(10), 20340–20358 (2013).
131. K. M. Dean et al., "Analysis of red-fluorescent proteins provides insight into dark-state conversion and photodegradation," *Biophys. J.* **101**(4), 961–969 (2011).
132. T. J. Wardill et al., "A neuron-based screening platform for optimizing genetically-encoded calcium indicators," *PLoS One* **8**(10), e77728 (2013).

Yi Shen undertook his PhD research with professor Robert E. Campbell in the Department of Chemistry at the University of Alberta, Edmonton, Canada. His research projects were focused on the development of new RFPs and RFP-based pH sensors.

Tiffany Lai is an MSc student at the University of Alberta, Edmonton, Canada. She earned her BSc from McGill University. Her research project focuses on the applications of ddFPs for life science research.

Robert E. Campbell is a professor of chemistry of the University of Alberta, Edmonton, Canada. He earned his BSc and PhD degrees from the University of British Columbia and undertook postdoctoral research at the University of California, San Diego. His research program focuses on the development of FPs and FP-based tools for live cell imaging. As of March 2015, plasmids developed in his lab have been requested more than 2900 times.